

Charge order in an interacting monolayer under transverse bias

Tim Ludwig and Carsten Timm

Institute of Theoretical Physics, Technische Universität Dresden, 01062 Dresden, Germany

(Received 18 July 2016; revised manuscript received 23 September 2016; published 28 October 2016)

A monolayer of molecules or quantum dots sandwiched between electrodes can be driven out of equilibrium by the application of a bias voltage between the electrodes. We study charge ordering, i.e., the spontaneous formation of a charge density wave, and the perpendicular current in such a system within a master-equation approach augmented by mean-field and classical Monte Carlo methods. Our approach is suitable for weak tunneling between the monolayer and the electrodes. For a square lattice with nearest-neighbor Coulomb repulsion, we present a comprehensive study of the zero-temperature phases controlled by the onsite energy, the bias voltage, and the degeneracy of the occupied single-site state. One of the most interesting results is the prediction of a conducting charge-density-wave phase that only occurs at a finite-bias voltage. We also study the universality classes of the phase transitions towards charge-ordered states at zero and nonzero temperatures. While all transitions at $T > 0$ and some at $T = 0$ belong to the two-dimensional Ising universality class, we also find an absorbing-to-active phase transition in the \mathbb{Z}_2 symmetric directed percolation (DP2) class at $T = 0$.

DOI: [10.1103/PhysRevB.94.155444](https://doi.org/10.1103/PhysRevB.94.155444)**I. INTRODUCTION**

Layers of quantum dots or single molecules sandwiched between conducting electrodes form promising systems for applications as well as for fundamental research. For the past 20 years, experimentalists have investigated the perpendicular current through self-organized layers of quantum dots in semiconductor systems [1–12]. These quantum-dot arrays were strongly disordered, though. Molecular layers offer at least two advantages: certain molecules readily form highly ordered self-assembled monolayers on semiconducting or metallic substrates [13–18] and individual molecules are, in principle, identical. On the other hand, it has proven to be difficult to fabricate a reliable second (top) contact. Novel methods, such as low-energy, indirect-path thermal evaporation [19], rolled-up nanomembranes [20–23], lift-off–float-on techniques [24–26], nanotransfer printing [27,28], and transfer of multilayer graphene [29] have been used to create reasonably homogeneous top contacts to molecular layers. Controlled contacts are a prerequisite for the application of molecular monolayers in electronic devices. Such applications are driven, on the one hand, by the trend to further miniaturization, and, on the other, by the possibility to functionalize the molecules [30].

Layers of molecules or quantum dots in sandwich structures also constitute model systems for nonequilibrium statistical physics: a bias voltage applied to the electrodes drives the system out of equilibrium. For time-independent bias, the system approaches a stationary state, which is characterized by a stationary current in the direction perpendicular to the monolayer. For noninteracting quantum dots or molecules, the individual entities conduct independently and the theoretical description can fall back on transport theory for single dots or molecules [31,32]. The case of interacting dots or molecules is much more interesting in that it combines interactions with driving. Such a system can show spontaneous symmetry breaking, begging the questions whether the corresponding phase transitions belong to a universality class that is known from equilibrium physics or to a genuinely nonequilibrium one [33–36].

In this paper, we study a relatively simple model in this class, namely, a square array of sites that are either empty or singly occupied due to a high charging energy and that interact through nearest-neighbor Coulomb repulsion. We allow for arbitrary (spin or orbital) degeneracy of the occupied states. The system is sandwiched between electrodes under an applied bias voltage. As we shall see, this nonequilibrium situation can induce spontaneous breaking of translational symmetry [34] by the formation of a charge density wave with ordering vector (π, π) , in which the two checkerboard sublattices have different average occupation. We employ a mean-field approximation in the framework of rate equations to obtain an overview of the possible phases, and classical nonequilibrium Monte Carlo simulations as an unbiased method to study them in more detail.

Our model is similar to the one studied by Kießlich *et al.* [37] and by Wetzler *et al.* [38], but their systems were relatively small or disordered. Their focus was on small arrays of quantum dots in semiconductor heterostructures, while we are interested in the statistical physics of clean systems in the thermodynamic limit. Leijnse [39] has more recently studied a square array without degeneracy. This work did not address the possibility of charge ordering and did not employ Monte Carlo simulations. A two-dimensional (2D) layer with interactions and hopping was studied within a Keldysh approach by Mitra *et al.* [40]. Their interest was in ferromagnetic order in the 2D layer and in the universality class of the nonequilibrium, voltage-driven phase transition.

The structure of this paper is as follows: In Sec. II, we define the model and methods. Section III gives a comprehensive discussion of the phases and phase transitions at zero temperature. Section IV presents results for nonzero temperatures. We give a summary in Sec. V.

II. MODEL AND METHODS

Our model consists of a 2D square lattice of quantum dots or molecules sandwiched between two conducting electrodes,

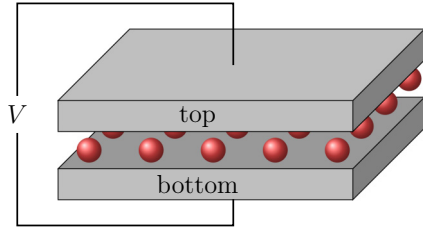


FIG. 1. Sketch of the model system, a square-lattice monolayer of quantum dots or molecules sandwiched between two conducting electrodes. A bias voltage V is applied between the electrodes.

as sketched in Fig. 1. The Hamiltonian $H = H_{\text{leads}} + H_{\text{layer}} + H_{\text{tun}}$ consists of the three terms

$$H_{\text{layer}} = E_d \sum_{i\sigma} \hat{n}_{i\sigma} + \frac{U_0}{2} \sum_i \sum_{\sigma \neq \sigma'} \hat{n}_{i\sigma} \hat{n}_{i\sigma'} + U_1 \sum_{(ij)} \sum_{\sigma\sigma'} \hat{n}_{i\sigma} \hat{n}_{j\sigma'}, \quad (1)$$

$$H_{\text{leads}} = \sum_{\alpha\mathbf{k}\sigma} (\varepsilon_{\mathbf{k}} - \mu_{\alpha}) a_{\alpha\mathbf{k}\sigma}^{\dagger} a_{\alpha\mathbf{k}\sigma}, \quad (2)$$

$$H_{\text{tun}} = \sum_{\mathbf{k}\sigma i\alpha} t_{\mathbf{k}i\alpha} a_{\alpha\mathbf{k}\sigma}^{\dagger} c_{i\sigma} + \text{H.c.}, \quad (3)$$

where E_d is the single-particle energy of the individual dots or molecules, U_0 is the onsite Coulomb interaction, U_1 is the nearest-neighbor Coulomb interaction, $\varepsilon_{\mathbf{k}}$ is the dispersion of electrons in the electrodes, μ_{α} is the chemical potential in electrode $\alpha = 1, 2$, and $t_{\mathbf{k}i\alpha}$ is the tunneling amplitude between the electrodes and the monolayer. For simplicity, the tunneling amplitude $\tilde{t} \equiv t_{\mathbf{k}i\alpha}$ and the density of states of the electrodes are assumed to be constant. $c_{i\sigma}$ is the electronic annihilation operator for a state in the monolayer at site i with quantum numbers σ , which could include the spin but, importantly, may also include an orbital index, and $\hat{n}_{i\sigma} \equiv c_{i\sigma}^{\dagger} c_{i\sigma}$ is the corresponding number operator. $a_{\alpha\mathbf{k}\sigma}$ is the annihilation operator for a state with spin σ and momentum \mathbf{k} in electrode α . We use U_1 as our unit of energy and measure E_d relative to the chemical potential in equilibrium. We consider the limit $U_0 \rightarrow \infty$ so that each site can only be empty or singly occupied. The voltage drop is assumed to be symmetric and the applied bias voltage is given by $eV = \mu_1 - \mu_2$.

The Hamiltonian for the layer, Eq. (1), does not contain intralayer hopping. For quantum dots, this situation is easily realized by making the separation between dots sufficiently large. On the other hand, molecular layers are typically closely packed. It is nevertheless possible to reduce the overlap between the relevant orbitals of neighboring molecules by choosing appropriate side groups. In the absence of wavefunction overlap and tunneling within the layer, the exchange interaction between different sites also vanishes and we are left with the direct Coulomb interaction in Eq. (1). The spin thus only enters by causing a twofold degeneracy. From a theoretical perspective, inclusion of intralayer hopping would transform the system into an extended Hubbard model out of equilibrium, a much more difficult problem. The methods we will discuss below rely on the decomposition of the

many-particle dynamics into single-site processes (coupled by their dependence on the occupation of neighboring sites). This would not be possible in the presence of intralayer hopping, which would instead require us to consider the many-body eigenstates of an extended Hubbard model.

The degeneracy of the occupied states, i.e., the number of possible realizations of an occupied site, is denoted by G , while we assume the unoccupied state to be nondegenerate. Hence, for L^2 lattice sites (L is the linear size of the system), there are $(G + 1)^{L^2}$ possible many-particle states. It is, however, advantageous to view the G occupied states as a single one and include the degeneracy factor G explicitly in the equations. The case of a single orbital per site, spin $\frac{1}{2}$, and vanishing magnetic field corresponds to $G = 2$. A strong magnetic field that shifts one spin orientation up to high energies would lead to $G = 1$. Orbital degeneracies and effective degeneracies due to vibrational modes [41–43] and local magnetic moments can result in larger values of G . Degeneracies of both the occupied and the unoccupied states are easily included and lead to the same results, except for overall constant factors, where G is now the ratio of the degeneracies of occupied and unoccupied states. A degeneracy of what we call the unoccupied state is naturally realized if the transition is not between an empty and a singly occupied orbital but between a singly occupied and a doubly occupied orbital. We conclude that it is meaningful to allow G to take any positive real value.

A. Master equation

For weak tunneling to the electrodes but strong interactions U_0 and U_1 , the master-equation formalism is most suitable [31,32,44,45]. The master equation is the equation of motion for the reduced density operator of the monolayer $\rho_{\text{red}} = \text{Tr}_{\text{leads}} \rho$, where ρ is the density operator of the whole system. In the limit of weak tunneling, a perturbative expansion in the tunneling amplitude \tilde{t} can be employed. The sequential-tunneling approximation is obtained by truncating this expansion after the second order. Furthermore, we make the standard assumption that the monolayer and the electrodes are in a product state with the electrodes in separate equilibrium at an early time $t_i \rightarrow -\infty$. By suitably organizing the expansion (or, alternatively, by a Markov assumption), we can make the resulting master equation local in time [44,45]. The result is the Wangsness-Bloch-Redfield master equation [46–48]

$$\frac{d\rho_{\text{red}}}{dt} = -i [H_{\text{layer}}, \rho_{\text{red}}(t)] - \int_0^{\infty} d\tau \text{Tr}_{\text{leads}} [H_{\text{tun}}, [e^{-i(H_{\text{layer}} + H_{\text{leads}})\tau} \times H_{\text{tun}} e^{i(H_{\text{layer}} + H_{\text{leads}})\tau}, \rho_{\text{red}}(t) \otimes \rho_{\text{leads}}^0]], \quad (4)$$

where ρ_{leads}^0 describes the initial equilibrium state of the electrodes and we have set $\hbar = 1$. We focus on the stationary state, which is obtained by setting $d\rho_{\text{red}}/dt = 0$. The result is a linear algebraic equation for ρ_{red} .

We employ the basis of occupation-number states in real space, i.e., of eigenstates of all number operators $\hat{n}_{i\sigma}$. The corresponding eigenvalues are denoted by $n_{i\sigma} = 0, 1$. These states are also eigenstates of H_{layer} . In this work, we assume that the stationary reduced density operator ρ_{red} is diagonal in

this basis, i.e., we will neglect all coherences. In the following, we discuss the conditions for this assumption to be valid.

First of all, coherences $\langle a|b\rangle$ between states with different total particle numbers N_a, N_b dephase nearly instantaneously due to superselection rules [49–51]. Such coherences are also seen to decouple from the diagonal components of ρ_{red} (i.e., the probabilities) and from the coherences between states with the same total particle number in Eq. (4). Coherences of the latter type do couple to the diagonal components and are generated with time even if they are not present in the initial state. The relevant processes involve the tunneling of an electron out of site i of the molecular layer into a typically adjacent site i' in electrode α and then back out of a site j' in the electrode into site j in the molecular layer (or in the opposite temporal order). Mathematically, they are controlled by the lesser and greater Green functions of lead electrons, which appear in the integral term of the master equation (4) [45]. In a clean system, the Green functions for states close to the chemical potential decay in real space as $\sin k_F r'/k_F r'$, where r' is the distance between points i' and j' in the electrode. This means that the terms generating nonlocal coherences are small if the distance between neighboring molecules, or more precisely between the points in the electrodes connected to neighboring molecules by tunneling, is large compared to the Fermi wavelength $\lambda_F = 2\pi/k_F$ in the electrodes. Moreover, in the presence of disorder in the leads, the Green functions are additionally cut off at the scale of the mean-free path l . We conclude that nonlocal coherences can be neglected if the separation between neighboring molecules is large compared to the Fermi wavelength or to the mean-free path in the electrodes.

This leaves the possibility of coherences between states that only differ by the local quantum numbers σ . Let us first consider the case that σ in Eq. (1) only refers to the z component of the real spin. It is easy to check that coherences between spin states decouple from the diagonal components if the full Hamiltonian H conserves spin. This means that such coherences are not generated if they are not present in the initial state and, moreover, decay to zero if there is any arbitrarily weak spin relaxation. This conclusion carries over to the case with σ containing additional (orbital) degrees of freedom: coherences can be neglected if H conserves the full set of quantum numbers σ . This, for example, applies to a model involving molecules with p_x and p_y (or d_{xz} and d_{yz}) orbitals where the interface is the xy plane. Tunneling only occurs to lead orbitals with the same mirror symmetries with regard to the xz and yz planes so that the pseudospin distinguishing between the two orbitals is conserved, in addition to the real spin.

If coherences are neglected, the master equation simplifies to rate equations for the probabilities $P_a \equiv \langle a|\rho_{\text{red}}|a\rangle$ of the many-body states $|a\rangle$ of the monolayer:

$$\frac{d}{dt} P_f = \sum_i (R_{i \rightarrow f} P_i - R_{f \rightarrow i} P_f). \quad (5)$$

In the sequential-tunneling approximation, the rates take the form [45,52,53]

$$R_{i \rightarrow f} = \sum_{\alpha} R_{i \rightarrow f}^{\alpha}, \quad (6)$$

with

$$\begin{aligned} R_{i \rightarrow f}^{\alpha} &= \frac{\tilde{t}^2 D}{h} \sum_j (G |c_j^{\dagger}|_{if}^2 f_{\alpha}(E_d + z_j U_1) \\ &\quad + |c_j|_{if}^2 [1 - f_{\alpha}(-E_d - z_j U_1)]) \\ &= \frac{\tilde{t}^2 D}{h} \sum_j (G |c_j^{\dagger}|_{if}^2 + |c_j|_{if}^2) f_{\alpha}(E_d + z_j U_1), \end{aligned} \quad (7)$$

where D is the density of states per electrode and spin, $f_{\alpha}(x) \equiv f(x - \mu_{\alpha})$ is the Fermi function $f(x)$, and $|c_j^{\dagger}|_{if}^2 \equiv |\langle f|c_j^{\dagger}|i\rangle|^2$. We have dropped the index σ because the rates do not depend on it and the degeneracy G is already included explicitly in the in-tunneling rates. Furthermore, we have used that sequential tunneling only connects many-body states $|i\rangle, |f\rangle$ that differ by a single electron at a single site j and only depends on the local energy contributions E_d and $z_j U_1$, where z_j is the number of occupied sites neighboring j .

It is easy to check that in the case of $V = 0$, i.e., for $\mu_1 = \mu_2$, the rates $R_{i \rightarrow f}$ satisfy detailed balance so that the system relaxes into its equilibrium state at the temperature of the electrodes. For $G = 1$ and $V = 0$, our system is equivalent to an Ising model in equilibrium. The role of the Ising magnetic field is played by the onsite energy E_d . The degeneracy G can be absorbed into this magnetic field as a temperature-dependent term, as we discuss below.

Our model satisfies a particle-hole symmetry. The symmetry operation consists of interchanging in-tunneling and out-tunneling processes and mapping the onsite energy according to $E_d \rightarrow -4U_1 - E_d$. For $G \neq 1$, the degeneracy of the *unoccupied* state becomes G after the mapping. At the level of the rate equations, this is equivalent to setting the degeneracy of the occupied state to $1/G$ and multiplying $\tilde{t}^2 D/h$ by G .

The staggered magnetization of an antiferromagnetic Ising model maps to $\langle n_A - n_B \rangle$, where n_A and n_B are the occupation numbers of any site on the checkerboard sublattices A and B , respectively. The brackets $\langle \dots \rangle$ denote the statistical average, over space and time, in the stationary state. Due to $U_0 \rightarrow \infty$, we have $0 \leq \langle n_{A,B} \rangle \leq 1$. We call $\langle n_A - n_B \rangle$ the checkerboard order parameter from now on. The corresponding susceptibility χ is

$$\chi \equiv \langle (n_A - n_B)^2 \rangle - \langle n_A - n_B \rangle^2. \quad (8)$$

Furthermore, we denote the total electron number in the molecular layer by N , the number of nearest-neighbor bonds of type $X \in \{00,01,10,11\}$, corresponding to empty-empty, empty-occupied, etc., by N_X , and the associated concentrations by $n = N/L^2$ and $n_X = N_X/L^2$. Lastly, the average current per site from the monolayer into the electrode α is given by

$$\langle I^{\alpha} \rangle = \frac{e}{L^2} \sum_{if} (N_f - N_i) R_{i \rightarrow f}^{\alpha} P_i, \quad (9)$$

where N_i (N_f) is the total electron number in the monolayer in the initial (final) state.

B. Mean-field approximation versus Monte Carlo simulations

We solve the rate equations (5) employing two complementary methods. First, we apply a mean-field approximation at

the level of probabilities (mean-field master equation, MFME). Specifically, we trace out all sites except for a single site j in the rate equations (5). The resulting probability for site j having the occupation number $n_j = 0, 1$ is $P_{n_j}^j \equiv \sum_{\{n_i=0,1 \mid i \neq j\}} P_{\vec{n}}$, where $\vec{n} = (n_1, \dots, n_{L^2})$ represents a many-body state of the whole layer in the occupation-number basis. The rate equations then take the form $dP_{n_j}^j/dt = F(P_{\vec{n}})$, where the right-hand side still depends on the full configuration. The main approximation then consists of the product ansatz $P_{\vec{n}} = \prod_j P_{n_j}^j$ in F . This approximation leads to coupled equations for the single-site probabilities $P_{n_j}^j$ for all sites j . Using $P_0^j + P_1^j = 1$, these are L^2 independent probabilities. To simplify the problem further, we only consider specific spatial variations of the probabilities $P_{n_j}^j$. Since we are interested in checkerboard order, we assume $P_{n_j}^j$ to be the same for all j on the same checkerboard sublattice A or B , i.e., $P_{n_j}^j = P_{n_A}^A$ for $j \in A$ and $P_{n_j}^j = P_{n_B}^B$ for $j \in B$. This only permits uniform and checkerboard-ordered solutions, where the uniform state corresponds to $P_n^A = P_n^B$. Since $P_0^s + P_1^s = 1$ for $s = A, B$, we have now reduced the problem to finding two unknowns P_1^A and P_1^B . The product ansatz constitutes a mean-field-type approximation since it replaces the spatial correlations included in $P_{\vec{n}}$ by much simpler ones that only depend on the averaged occupation on each sublattice. This approximation goes beyond a Hartree approximation, which would replace the nearest-neighbor Coulomb interaction by the interaction with the average charge density. Here, we retain the information that the sites are always either occupied or unoccupied.

The resulting equation of motion for the probability of a site on sublattice $s = A, B$, here denoted as site 0, having the occupation n_0 reads as

$$\begin{aligned} \frac{dP_{n_0}^s}{dt} &= \sum_{n_1, \dots, n_4} (R_{|\vec{n}_0, z_0\rangle \rightarrow |n_0, z_0\rangle} P_{\vec{n}_0}^s - R_{|n_0, z_0\rangle \rightarrow |\vec{n}_0, z_0\rangle} P_{n_0}^s) \\ &\quad \times P_{n_1}^{\bar{s}} \dots P_{n_4}^{\bar{s}}. \end{aligned} \quad (10)$$

In deriving this equation, we have used that under sequential tunneling only the occupation number of a single site changes. The transition rate for this process depends on whether an electron tunnels in or out and on the number of occupied neighboring sites. We can thus parametrize the rates $R_{|n_0, z_0\rangle \rightarrow |\vec{n}_0, z_0\rangle}$ by the initial and final occupation numbers n_0 and $\vec{n}_0 \equiv 1 - n_0$, respectively, and the number $z_0 \equiv \sum_{i=1}^4 n_i$ of occupied neighboring sites on the square lattice, enumerated by i . In Eq. (10), $\bar{s} = B, A$ for sublattice $s = A, B$ since the neighboring sites are always on the other sublattice. Here and in the following, we use $|n_j, z_j\rangle$ as a shorthand notation for the full many-body state $|n_1, n_2, \dots\rangle$, which highlights the quantities that affect the sequential tunneling at site j . Stationary states are fixed points, which are obtained by setting the time derivatives to zero. We solve the equations numerically, discarding any unstable fixed points. We note that this procedure is different from the one used in Ref. [39], which is formulated in terms of the conditional occupation probabilities of the sites, depending on the occupation of their neighbors.

Second and foremost, we use Monte Carlo simulations. While they are numerically more expensive, they have the

advantage of being free from approximations beyond those made in the derivation of the sequential-tunneling rate equations (5), apart from finite-size effects. Moreover, the solutions are not restricted to uniform or checkerboard order. As the system size is finite, we have to evaluate the average $\langle |n_A - n_B| \rangle$ instead of $\langle n_A - n_B \rangle$. We consider linear system sizes L between 16 and 16384 and periodic boundary conditions.

The straightforward algorithm for local updates is the following: randomly choose a site j . If this site is initially occupied (unoccupied), the only possible transition is to the unoccupied (occupied) state. Calculate the rate $R_j \equiv R_{i \rightarrow f}$ for this transition from Eqs. (6) and (7); the result depends on the occupations of the neighboring sites. Accept the transition with the probability $R_{i \rightarrow f} / \max(R)$, where $\max(R) = 2G\tilde{\tau}^2 D/h$ is the maximum possible rate.

This algorithm is highly inefficient if the rate R_j chosen as described above often turns out to be small compared to $\max(R)$ since then many Monte Carlo steps are rejected. Hence, we instead employ the rejection-free update scheme described in the following. First, note that there are only 10 distinct local updates in sequential tunneling, which are enumerated by the initial occupation $n_j = 0, 1$ and the number of occupied neighbors $z_j = 0, \dots, 4$. We first randomly select one of the 10 update types with the proper branching fraction $\tilde{R}_{n_j, z_j} / \sum_{n_k, z_k} \tilde{R}_{n_k, z_k}$, which is determined from the total rates of processes of each of the types $\tilde{R}_{n_j, z_j} \equiv R_{|n_j, z_j\rangle \rightarrow |\vec{n}_j, z_j\rangle} \sum_p \delta_{n_p, n_j} \delta_{z_p, z_j}$, where p enumerates the sites of the system. These quantities are easily updated in each Monte Carlo step. Then, we randomly choose a site with occupation n_j and z_j occupied neighbors. This step is rejection free since the program keeps lists of all sites that are in each of the 10 states $|n_j, z_j\rangle$. Lastly, we update this site and advance the simulation time by the average waiting time $1 / \sum_{n_k, z_k} \tilde{R}_{n_k, z_k}$ [54]. This algorithm is related to the one introduced by Bortz *et al.* [55] and independently by Gillespie [56], and further improved by Schulze [57]. We measure all times in units of $t_0 \equiv h/(\tilde{\tau}^2 D)$, which is the average waiting time between two tunneling events at a single site if the transition is inside the bias window and $T = 0$ and $G = 1$. To our knowledge, more efficient update algorithms, such as cluster updates [58,59], do not exist for the rates in Eq. (6), which do not satisfy detailed balance.

III. RESULTS FOR ZERO TEMPERATURE

In the limit of zero temperature, the Fermi distribution becomes a step function and thus the rates change discontinuously. Consequently, the stationary state is the same for all values of E_d and eV within each of the regions defined in Fig. 2. This allows us to give a complete discussion of all possible stationary states. The regions are labeled by the numbers of transition energies below the chemical potentials of the two electrodes. As an example, Fig. 3 shows the relevant energies for the region (4,1): four transitions lie below the chemical potential of the top electrode but only one transition lies below the chemical potential of the bottom electrode.

To get an overview, we present in Fig. 4 the MFME phase diagram for the case $G = 2$. We find all possible combinations of phases with and without checkerboard charge order and with and without a charge current through the monolayer.

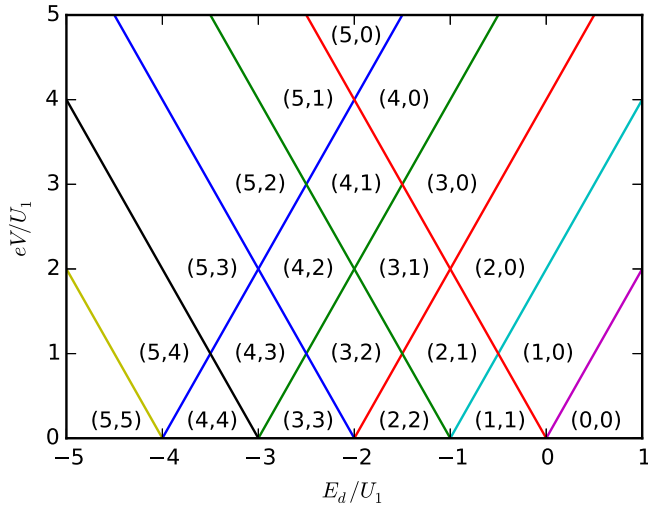


FIG. 2. Crossings of the transition energies of the square-lattice monolayer and the chemical potentials of the electrodes, as functions of the onsite energy E_d and the bias voltage V . In the limit $T \rightarrow 0$, the transition rates $R_{i \rightarrow j}$ are constant within each region. The labels (m, n) specify the numbers of transition energies below the chemical potentials m for the top electrode 1 and n for the bottom electrode 2.

In the presence of checkerboard order, the MFME has two stationary solutions, which are related by interchanging the two sublattices. In the region labeled “coexistence,” the stationary MFME has both checkerboard blocked and uniform conducting solutions. In the following, we discuss each phase based on rigorous results and Monte Carlo simulations.

A. Uniform conducting phase at large bias

For fixed onsite energy E_d and sufficiently high bias voltage V , the system is always in the region (5,0) (see Fig. 2). In this regime, an analytical solution of the rate equations (5) is possible. Since the in-tunneling and out-tunneling rates are independent of the occupation numbers of the neighboring

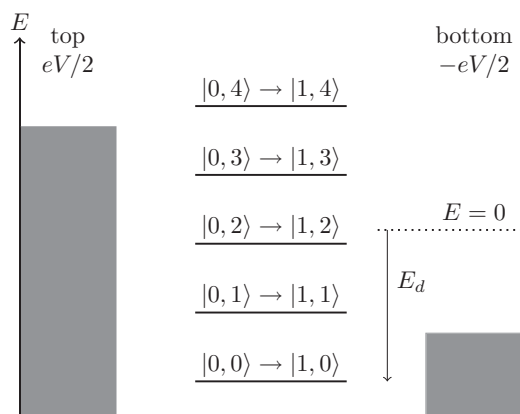


FIG. 3. Sketch of the chemical potentials and the transition energies for in-tunneling processes for the region (4,1) of Fig. 2. $|n_j, z_j\rangle$ denotes a many-particle state for which the site j involved in the tunneling has occupation number n_j and z_j occupied neighbors (all other occupation numbers are irrelevant for this process and are suppressed).

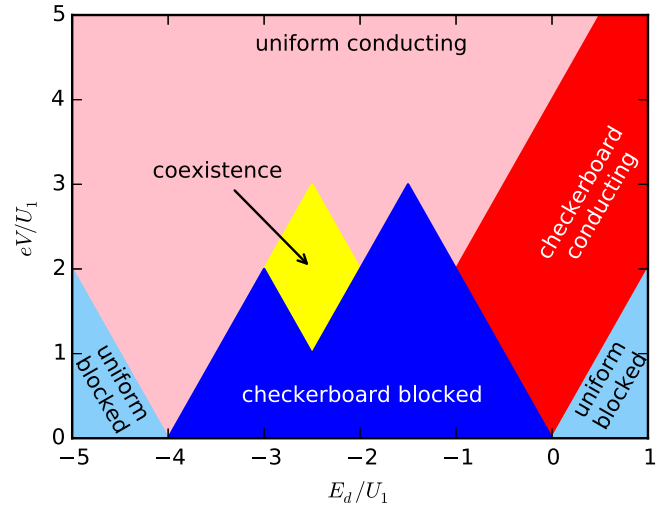


FIG. 4. Phase diagram obtained from the MFME for a monolayer with degeneracy $G = 2$ and temperature $T = 0$. The phases for negative bias voltage, $eV/U_1 < 0$, are the mirror image of the phases shown. The terms “uniform” and “checkerboard” refer to the checkerboard order parameter $\langle n_A - n_B \rangle$, where n_A and n_B are the occupation numbers per site on sublattices A and B , respectively. This order parameter is zero (nonzero) in the uniform (checkerboard) phases. The term “conducting” (“blocked”) characterizes phases that carry (do not carry) a current through the monolayer. In the region labeled “coexistence,” checkerboard blocked and uniform conducting stationary states coexist.

sites, the dynamics of the individual sites is decoupled. In the stationary state, the probabilities of a site j being occupied or unoccupied are $P(n_j = 0) = 1/(G + 1)$ and $P(n_j = 1) = G/(G + 1)$, respectively. These are the same values one finds for the equilibrium ($V = 0$) state in the limit $T \rightarrow \infty$. The average current per site is $\langle I^1 \rangle = eD\tilde{t}^2G/h(G + 1)$. The system is clearly in the uniform conducting phase. The solution of the rate equations (5) is given by the product of the aforementioned single-site probabilities since the sites are decoupled.

B. Quasiequilibrium, blocked phases

All regions connected to the zero-bias line, i.e., the regions (m, m) and $(m + 1, m)$ in Fig. 2, can be mapped onto an equilibrium Ising-type model with degeneracy G of one of the states and an applied magnetic field, as we show in the following. The equilibrium Ising model with $G = 1$ has of course been investigated thoroughly [60–62]. The mapping between our monolayer Hamiltonian and the Ising Hamiltonian

$$H_{\text{Ising}} = -J \sum_{\langle ij \rangle} S_i S_j - B \sum_i S_i \quad (11)$$

reads as

$$S_i = 2n_i - 1 = \pm 1, \quad (12)$$

$$J = -U_1/4, \quad (13)$$

$$B = -E_d/2 - U_1. \quad (14)$$

The state $S_i = +1$ has degeneracy G .

We first consider the regions (m, m) , which contain parts of the line $eV/U_1 = 0$. Recall that the $T = 0$ stationary state is the same throughout each region. It is thus sufficient to investigate the case $eV/U_1 = 0$, which corresponds to the model in equilibrium, in the limit $T \rightarrow 0$. But, this state is just the ground state of H_{Ising} . For $E_d/U_1 < -4$, this is the fully occupied state. For $-4 < E_d/U_1 < 0$, there are two degenerate ground states with checkerboard charge order with one sublattice occupied and the other unoccupied. Finally, for $E_d/U_1 > 0$ the ground state is completely empty. The degeneracy G is irrelevant in these cases since the energy of the microstates does not depend on it. The corresponding currents [Eq. (9)] vanish in all these regions since all transition rates out of the respective ground states go to zero for $T \rightarrow 0$ [63].

Next, we turn to the regions $(m+1, m)$, which touch the line $eV/U_1 = 0$ at a single point. While the stationary state is still the same throughout each of these regions, the equilibrium state now lies at a corner of the region, which may be distinct from its interior. These corner points at $V = 0$ have fine-tuned values of $E_d/U_1 = -4, -3, -2, -1, 0$ (see Fig. 2), and correspond to one transition energy being resonant with the chemical potential, which is the same for both electrodes. One can see from Eq. (7) that the rates in the interior, i.e., for $V \neq 0$, and at the corner, i.e., for $V = 0$, have the same limit for $T \rightarrow 0$. This result relies on the symmetric coupling to the electrodes: For $V = 0$, the Fermi functions involving the resonant transition approach $\frac{1}{2}$ for both electrodes in the limit $T \rightarrow 0$, whereas for $V \neq 0$, one of them approaches unity and the other zero. Since for symmetric coupling only their sum enters, the results are the same. For the regions (2,1), (3,2), and (4,3), the stationary states are thus identical to the ground states for fine-tuned onsite energies $E_d/U_1 = -1, -2$, and -3 , respectively. However, these ground states are not different from the rest of the range $-4 < E_d/U_1 < 0$: they are the two states with checkerboard order. The current again vanishes, by the same argument as above. The regions (1,0) and (5,4) are special in that their corner points at $V = 0$ lie right on the transition between different ground states. We will investigate these cases in Sec. III C.

In summary, in the regions (1,1), (2,1), (2,2), (3,2), (3,3), (4,3), and (4,4) we find checkerboard charge order and vanishing current, in agreement with the MFME phase diagram in Fig. 4. This phase can be understood in terms of Coulomb blockade due to the nearest-neighbor repulsion U_1 . In the region (5,5), the sites are fully occupied and the current vanishes. This is the Coulomb-blockade regime due to the onsite repulsion U_0 . Finally, in the region (0,0) we find an empty lattice and vanishing current.

C. Degeneracy-driven phase transitions in the conducting phases

We now consider the regions (1,0), (2,0), (3,0), and (4,0) and their particle-hole-symmetry partners (5,4), (5,3), (5,2), and (5,1) in Fig. 2. The regions (1,0) and (5,4) are interesting since the discussion in Sec. III B suggests that their stationary states inherit properties from an equilibrium Ising model fine tuned to its critical point. Moreover, for the region (1,0) [as well as (2,0)] the MFME for $G = 2$ predicts a state with checkerboard charge order that is nevertheless conducting

(see Fig. 4). On the other hand, the state in region (5,4) is uniform and conducting, according to the MFME. Since the region (5,4) with degeneracy G is equivalent to the region (1,0) with degeneracy $1/G$ by a particle-hole transformation, the MFME results imply the existence of a phase transition between uniform and checkerboard states as a function of G . Indeed, by determining the stationary state of the MFME for various G , we find the critical degeneracy $G_c \approx 1.054$. It is then interesting to characterize this phase transition without making a mean-field approximation. In particular, we want to determine its universality class.

Before turning to the simulations, we first present an analytical estimate for the critical degeneracy G_c for the region (1,0). The critical value for the region (5,4) is then just $1/G_c$. As noted in Sec. III B, in the limit $T \rightarrow 0$ the rates in the interior of region (1,0) are the same as at the corner point $eV/U_1 = 0, E_d/U_1 = 0$. The critical value G_c can be related to the critical magnetic field B_c of an antiferromagnetic Ising model. We set $k_B = 1$ and consider the partition function $Z = \sum_a G^{N_a} e^{-E_a/T}$, where E_a is the energy of microstate $|a\rangle$ and N_a is the number of occupied sites in this microstate. The energy is given by $E_a = N_a E_d + Z_a U_1$, where Z_a is the number N_{11} of bonds between two occupied neighboring sites in microstate $|a\rangle$. The partition function can be written as

$$Z = \sum_a \exp\left(-\frac{N_a(E_d - T \ln G) + Z_a U_1}{T}\right). \quad (15)$$

According to Eq. (14), the Ising magnetic field is now $B = -(E_d - T \ln G)/2 - U_1$. At the corner point of the region (1,0), we have $E_d = 0$. The equivalent Ising model shows a phase transition between checkerboard and uniform order as a function of magnetic field. The critical field $|B| = B_c$ is determined by the temperature T and the coupling constant $J = -U_1/4$. Taking into account that B is negative for small T , we can then write the critical degeneracy as

$$G_c(U_1, T) = \exp\left(\frac{-2B_c(U_1, T) + 2U_1}{T}\right). \quad (16)$$

This expression is exact but, to the best of our knowledge, the analytical form of the function B_c is not known [61,64]. The conjectured low-temperature expansion proposed by Müller-Hartmann and Zittartz [61], $B_c \cong 4|J| - T \ln 2 = U_1 - T \ln 2$, gives $\lim_{T \rightarrow 0} G_c = e^{2 \ln 2} = 4$.

The above discussion is based on the mapping to an equilibrium Ising model. This is not possible for the regions (2,0) and (3,0), which should, however, be physically similar to (1,0) since all out-tunneling transitions are energetically possible while only some in-tunneling transitions are allowed. [The region (4,0) will be discussed below.] We have performed Monte Carlo simulations to study the degeneracy-driven transition in these regions. Figure 5 shows the checkerboard order parameter raised to the power 8 and the corresponding susceptibility to the power $-\frac{4}{7}$. For all three regions (1,0), (2,0), and (3,0), we find a transition to checkerboard order for increasing degeneracy G . The critical degeneracy $G_c \approx 3.6$ for the region (1,0) is slightly smaller than the value of $G_c \approx 4$ based on the low-temperature expansion of Ref. [61]. On the other hand, the MFME prediction $G_c \approx 1.054$ is clearly much too small. Indeed, for the case of $G = 2$ with pure spin

degeneracy, our simulations do not find checkerboard order in any conducting region, in contrast to the MFME phase diagram in Fig. 4.

Figure 5 shows some finite-size effects, in particular in the susceptibility. Nevertheless, the transitions in the regions (1,0), (2,0), and (3,0) are consistent with critical exponents of $\frac{1}{8}$ for the order parameter and $-\frac{4}{7}$ for the susceptibility, respectively, and thus with 2D Ising critical behavior [60]. The nonequilibrium transition is indeed expected to belong to the classical 2D Ising universality class based on the arguments of Ref. [40]: integrating out the microscopic degrees of freedom, one obtains a description in terms of a classical field coupled to noise. Generically, the spectrum of this noise is nonzero in the zero-frequency limit, which corresponds to the Ising universality class (“model A” in the terminology of Hohenberg and Halperin [33]). Newer works show that this is indeed true for a scalar (Ising) model, such as ours, but not for multicomponent order parameters [65].

Moreover, G_c increases with increasing bias voltage V , i.e., from region (1,0) to (2,0) and even more to (3,0). This dependence can be understood as follows: For a perfect

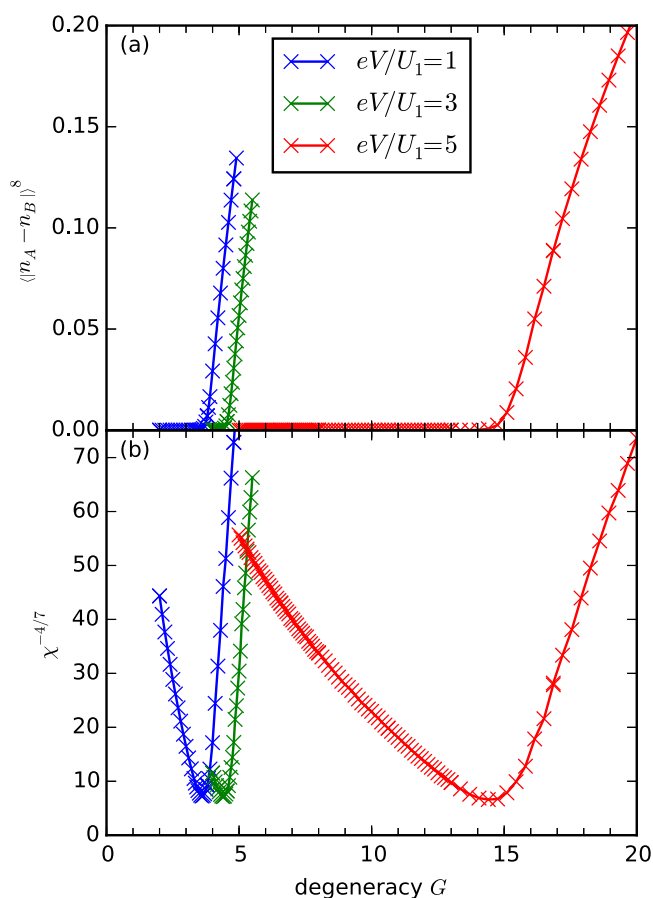


FIG. 5. Monte Carlo results for (a) the checkerboard order parameter $\langle |n_A - n_B| \rangle^8$ and (b) the corresponding susceptibility to the power $-\frac{4}{7}$ as functions of the degeneracy G of the occupied states. The values $eV/U_1 = 1, 3, 5$ correspond to the regions (1,0), (2,0), and (3,0) in Fig. 2, respectively. The remaining parameters are $T/U_1 = E_d/U_1 = 0$ and $L = 64$. The results are consistent with the 2D Ising universality class.

checkerboard-ordered state, a current flows through the occupied sublattice, as the out-tunneling transition is in the bias window. In contrast, the in-tunneling transition needed to fill a site on the empty sublattice, i.e., to create an occupied defect, is forbidden, except when there are enough empty defects at the surrounding sites on the occupied sublattice. Raising the bias voltage lowers the required number of empty defects and thus makes it easier to destroy the checkerboard order. On the other hand, raising G increases the in-tunneling rate for filling an empty site, i.e., for removing an empty defect, which stabilizes the order [66].

In the region (4,0), checkerboard order is even more strongly destabilized than in the previous cases since an occupied defect on the empty sublattice is possible as soon as one empty defect on the occupied sublattice exists. Furthermore, the average concentration of empty defects on the occupied sublattice is high since the out-tunneling transition is in the bias window. This concentration is suppressed by a large G but at the same time the creation rate for occupied defects neighboring an empty defect is enhanced. The latter effect evidently prevents charge order even at large G . Our simulations do not show any sign of a transition for G up to 10^8 .

The regions (5,4), (5,3), (5,2), and (5,1) are related to the regions (1,0), (2,0), (3,0), and (4,0), respectively, by interchanging empty and occupied states and replacing G by $1/G$. This means that degeneracy-driven transitions in regions (5,4), (5,3), and (5,2) take place at critical values $G_c < 1$, which correspond to higher degeneracy of the empty state compared to the occupied state of a single site (see the discussion of G in Sec. II).

D. Absorbing phase transitions

We now turn to the three diamond-shaped regions highest in the bias voltage, i.e., regions (3,1), its particle-hole-symmetry partner (4,2), and (4,1) in Fig. 2. In all three and indeed in all regions (m,n) with $m < 5$ and $n > 0$, the rates for the transitions $|1,0\rangle \rightarrow |0,0\rangle$ and $|0,4\rangle \rightarrow |1,4\rangle$ both vanish (for the notation $|n_j, z_j\rangle$, see Fig. 3). Consequently, there are no allowed transitions out of the perfect checkerboard states. This is the defining property of *absorbing* states [35,36]. Absorbing states are necessarily stationary, but for an infinite system it is possible that the stationary state approached from nearly all (namely, all except for a fraction that vanishes in the thermodynamic limit) initial states is not one of the absorbing states. Such a nonabsorbing stationary state is called *active*. If an active state only exists in part of the parameter range, then an absorbing-to-active phase transition has to occur [35,36].

Our Monte Carlo simulations suggest that the stationary state in regions (3,1) and (4,2) is an absorbing checkerboard state for $G = 1$ but is a uniform, and thus active, state in the region (4,1). However, the results have to be analyzed with care since for any finite system, the simulation will eventually end up in one of the absorbing states, possibly after a very long time.

To check that the regions really lie on different sides of an absorbing phase transition, it is desirably to tune continuously through the purported transition. In addition, this would allow us to determine its universality class. However, the naive idea

of fixing the temperature T to a small nonzero value and tuning the bias voltage V does not work since at $T > 0$ the transitions out of the perfect checkerboard states occur with nonzero rates so that these states are no longer absorbing. Instead, we define $\Delta V \equiv V - V_c$, where V_c is a bias voltage on the boundary between the regions (4,1) and (3,1) for a suitably chosen E_d . The boundary between regions (4,1) and (4,2) is analogous. The rates $R_{|0,4\rangle \rightarrow |1,4\rangle}$ and $R_{|1,0\rangle \rightarrow |0,0\rangle}$, which make the checkerboard state nonabsorbing, are then proportional to the Fermi function $f(U_1 + \Delta V)$. These rates are tuned to zero by letting $T \rightarrow 0$. On the other hand, the rates $R_{|0,1\rangle \rightarrow |1,1\rangle}$ and $R_{|1,1\rangle \rightarrow |0,1\rangle}$ are proportional to $f(\Delta V)$ and are kept constant by taking $\Delta V \rightarrow 0$ while keeping $\Delta V/T$ fixed.

Now, being able to tune our system continuously by changing $\Delta V/T$, we use a dynamical-scaling analysis [35,67–70] to clarify the occurring phases and transitions. Two standard critical exponents of an absorbing phase transition are defined by the scaling relations [35,70]

$$P_{\text{surv}} \sim t^{-\delta}, \quad (17)$$

$$\rho_{\text{act}} \equiv n_{00} + n_{11} \sim t^{\Theta} \quad (18)$$

for large times t . They pertain to a system prepared in an initial state that differs from an absorbing (checkerboard) states by a localized defect. P_{surv} is the survival probability, i.e., the probability that the system does not reach an absorbing state until the time t , and $\rho_{\text{act}} = n_{00} + n_{11}$ is the density of active sites [35], which in our model correspond to empty-empty and occupied-occupied nearest-neighbor bonds. Note that both exponents are free from finite-size effects since in our simulations the lattice was always larger than any grown cluster of active sites.

We concentrate on simulations for $G = 1$. Figure 6 shows results for P_{surv} . Since the exponent δ is close to unity, we have plotted P_{surv} multiplied by t/t_0 . Figure 7 shows results for $\rho_{\text{act}} = n_{00} + n_{11}$. We find a clear transition at $\Delta V/T \approx -3.49$ that agrees with the 2D \mathbb{Z}_2 symmetric directed-percolation universality class (DP2) [35,71,72]. Dornic *et al.* [73] conjecture that transitions with two symmetric absorbing states belong to the universality class of the generalized voter model. The latter has an upper critical dimension of two so that one expects mean-field exponents $\delta = 1$ and $\Theta = 0$ with logarithmic corrections [71,72]. Previous work supports either mean-field behavior with logarithmic corrections or exponents rather close to the mean-field ones [71,72], where the best estimate is $\delta = 0.900(15)$ and $\Theta = -0.100(25)$ [71].

While our focus is not on this debate, we briefly comment on the critical behavior. If P_{surv} followed mean-field scaling with logarithmic corrections, Fig. 6(a) would show a straight line for large t , at the critical value of $\Delta V/T$. If P_{surv} instead satisfied the power law (17), Fig. 6(b) would show a straight line. Similarly, Fig. 7(a) [Fig. 7(b)] would show a straight line at the critical $\Delta V/T$ if $n_{00} + n_{11}$ showed mean-field scaling with logarithmic corrections (power-law scaling). While $t P_{\text{surv}}$ in Fig. 6 appears to depend logarithmically on t for small t [note the straight line in Fig. 6(a)], P_{surv} crosses over to pure mean-field scaling with exponent $\delta = 1$ and without logarithmic corrections for $t/t_0 \gtrsim 10^4$ (horizontal line in both panels for $\Delta V/T = -3.4910625$). On the other hand,

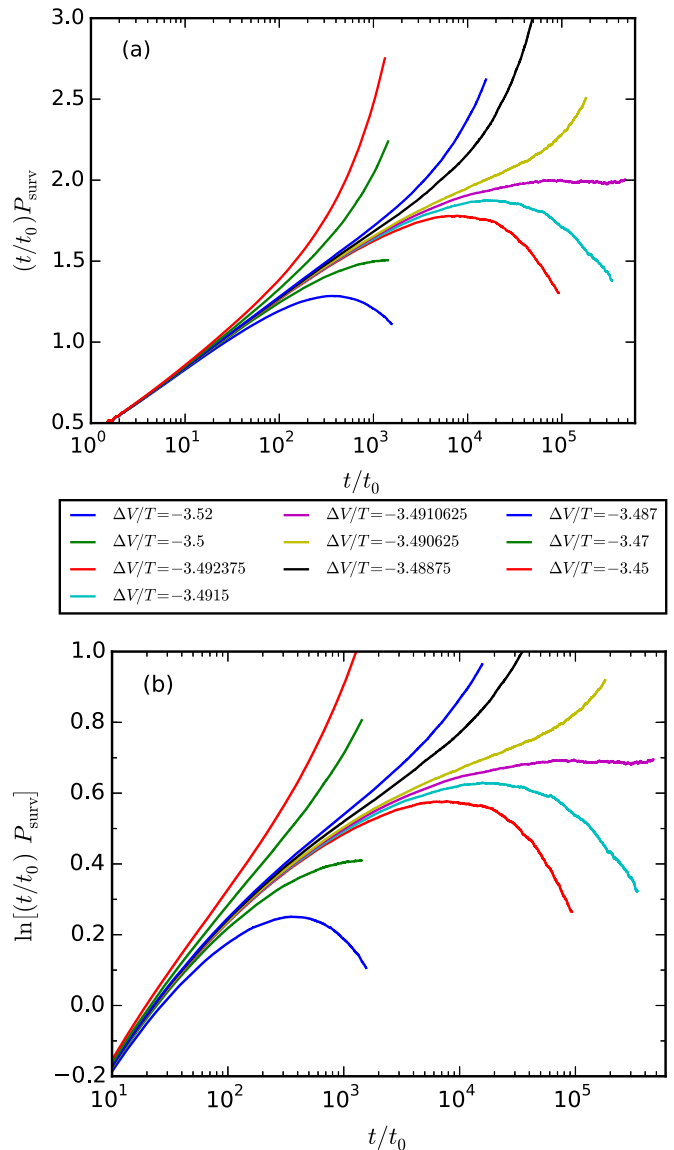


FIG. 6. Survival probability P_{surv} multiplied by t/t_0 in (a) single- and (b) double-logarithmic plots. The results have been obtained from Monte Carlo simulations for $G = 1$ and various values of $\Delta V/T$ (see text), starting with a single site deviating from the checkerboard state. The unit of time is $t_0 \equiv h/(\tilde{t}^2 D)$.

the scaling of $n_{00} + n_{11}$ shown in Fig. 7 does not clearly discriminate between the two scaling forms. The data for $\Delta V/T = -3.4910625$ are not consistent with the mean-field exponent $\Theta = 0$ without logarithmic corrections, i.e., with $n_{00} + n_{11} = \text{const}$, for $t/t_0 > 10^5$, unlike in Fig. 6. We suggest that either the large- t scaling regime has not been reached in our simulations or the corrections are more complicated than a simple logarithm $\ln(t/t_0)$.

To check the critical behavior further, we have investigated the time evolution of the concentration $\rho_{\text{act}} = n_{00} + n_{11}$ of active sites, i.e., of empty-empty and occupied-occupied bonds, when we start from a completely empty or completely occupied lattice, in which *all* bonds are active. In this case, the mean-field plus logarithmic form of the scaling relation at

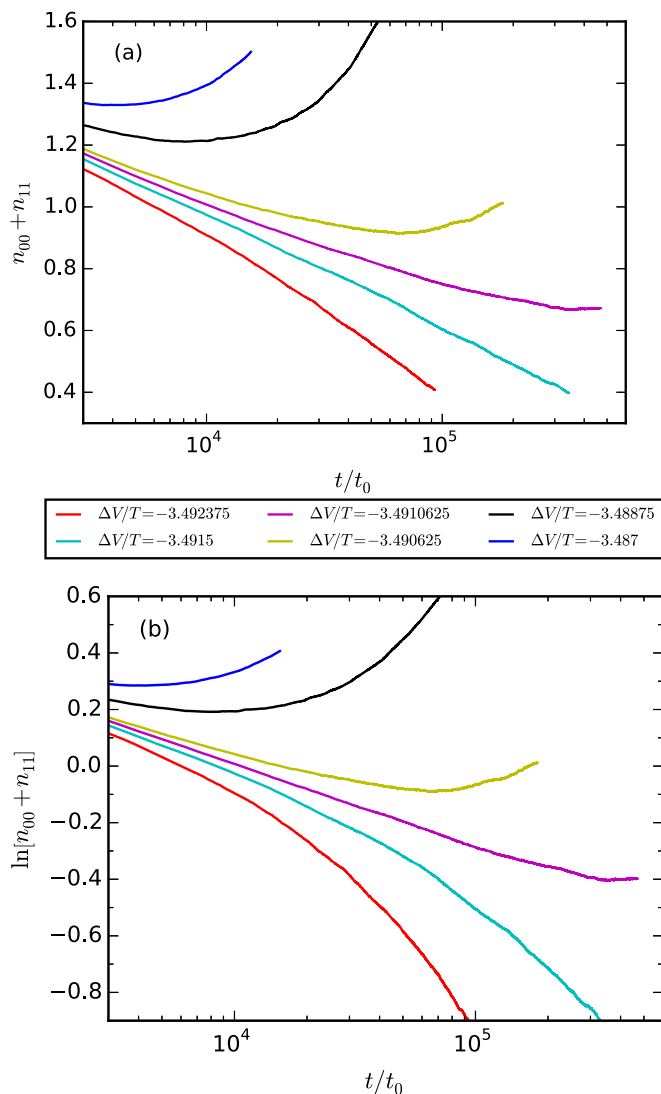


FIG. 7. Concentration of active bonds vs time t/t_0 in (a) single- and (b) double-logarithmic plots. The results have been obtained from Monte Carlo simulations for $G = 1$ and various values of $\Delta V/T$ (see text), starting with a single site deviating from the checkerboard state.

criticality reads as

$$n_{00} + n_{11} \sim \frac{1}{\ln t}, \quad (19)$$

whereas the power-law form is

$$n_{00} + n_{11} \sim t^{-\alpha}, \quad (20)$$

where the best estimate is $\alpha = 0.080(4)$ [71]. Our results are presented in Fig. 8. Figure 8(a) [8(b)] would show a straight line at the critical $\Delta V/T$ if $n_{00} + n_{11}$ satisfied mean-field plus logarithmic (power-law) scaling. The data agree better with mean-field scaling with logarithmic corrections for smaller t but do not exclude a crossover to power-law scaling at larger times.

In any case, while we cannot resolve the critical behavior, the transition between regions (4,1) and (3,1) shows clear characteristics of the 2D DP2 universality class. This is reasonable since a key feature of DP2 is the existence of

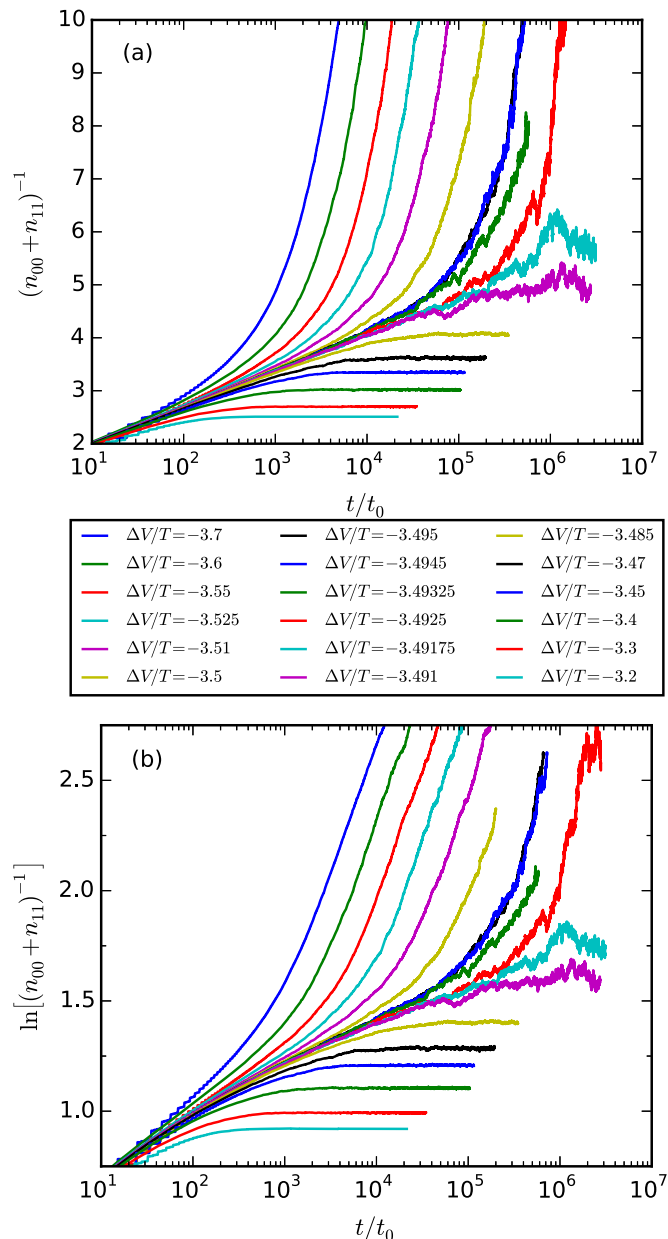


FIG. 8. Inverse of the concentration of active bonds vs. time t/t_0 in (a) single- and (b) double-logarithmic plots. The results have been obtained from Monte Carlo simulations for $G = 1$ and $L = 8192$ and various values of $\Delta V/T$ (see text), starting with an empty lattice, which corresponds to all bonds being active.

two symmetry-related absorbing states. Our model obviously has two absorbing checkerboard states that are related by a lattice translation. The DP2 character of the transition supports our conclusion that the system in region (4,1) is in the active, uniform state, whereas in region (3,1) it is in the absorbing, checkerboard state. It is interesting that we find a DP2 transition in view of the expectation that the nonequilibrium phase transitions of our model are generically of Ising type [40,65]. We conjecture that this is made possible by the fine tuning inherent in taking ΔV and T to zero with $\Delta V/T$ fixed.

The question arises as to whether the system in the regions (3,1), (4,2), and (4,1) can be driven across the DP2 absorbing phase transition by varying G . Increasing G favors occupied over empty sites. We would thus expect it to destabilize checkerboard order in favor of a uniform state with occupancy close to unity. Since region (4,1) is in the active phase even for $G = 1$ we do not expect the active phase to be destroyed for any G . Indeed, we have not found any sign of checkerboard order for G values up to 10^8 .

We now turn to the regions (4,2) and (3,1), in which a DP2 transition as a function of G might occur. We present simulation results for the surviving concentration $n_{00} + n_{11}$ of active bonds for a fully occupied (hence, active) starting configuration in Fig. 9. There is no indication of a phase transition for G up to 10^6 . Note that the time evolutions shown in Fig. 9 sometimes get trapped in a seemingly stationary state with nonzero active sites. These states consist of an even number of straight domain walls of the checkerboard order spanning the finite, periodic system. These domain walls are very long lived under local updates since their annihilation

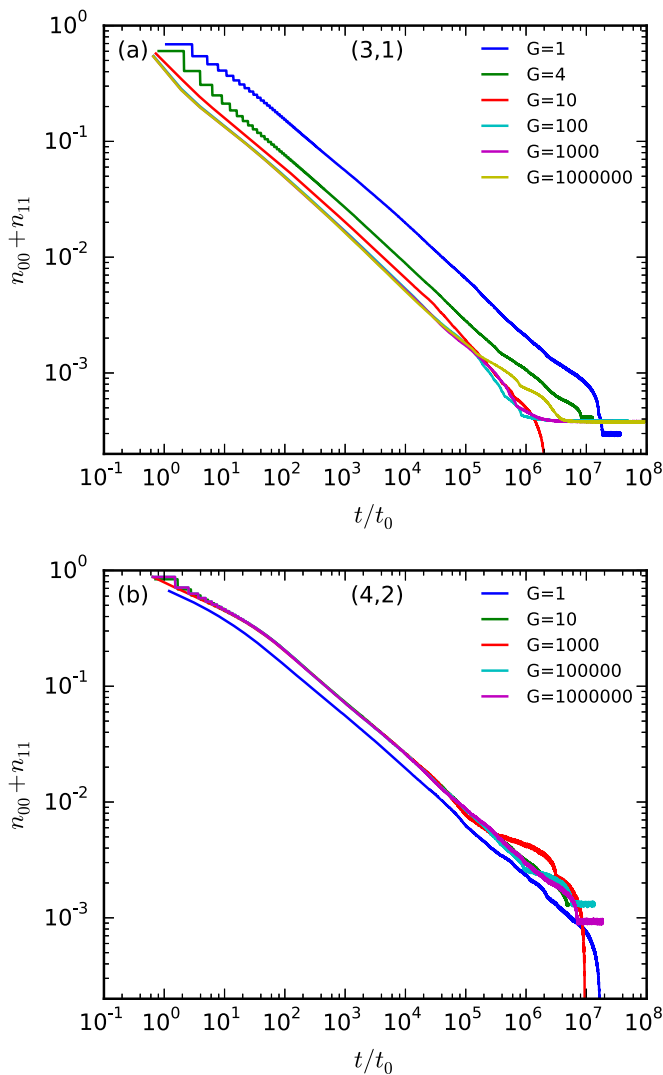


FIG. 9. Concentration of active sites for (a) region (3,1) and (b) region (4,2), from Monte Carlo simulations starting with a fully occupied lattice, for $L = 8192$, $T/U_1 = 0$, and various values of G .

requires them to first deform and reconnect. They clearly would not be possible in an infinite system. Thus, we conclude that the regions (4,2) and (3,1) are in the absorbing phase for all G . In particular, the coexistence regime found in the MFME phase diagram in Fig. 4 does not exist, only the checkerboard blocked phase is stable here. This general result is further supported by the power-law decay of $n_{00} + n_{11}$ with time, in the limit of large t but before finite-size effects occur, with an exponent of approximately $\frac{1}{2}$. This behavior was previously interpreted as being characteristic for the absorbing regime [73].

E. Phase diagram, occupation, and current

In the previous subsections, we have discussed the stationary state at $T = 0$ for all the regions in Fig. 2. The results are summarized in the phase diagram in Fig. 10, which partially anticipates results for the current that are presented below. We mention in passing that, although the simulations are not restricted to uniform and checkerboard-ordered phases, we did not find any other type of charge order. One of the most intriguing results is the possibility of *bias-induced charge order*: consider for example an onsite energy $E_d > 0$. If the degeneracy G is sufficiently large and we increase the bias voltage V starting from zero, the system is initially in a uniform blocked phase with all sites empty. But, at $eV = 2E_d$ it enters a conducting phase with checkerboard charge order (see Sec. III C). At a higher bias, there is a second transition towards a uniform conducting phase.

While the applied bias voltage V is easily varied, this is not the case for the onsite energy E_d . One could, however, prepare series of devices with different onsite energies. In molecular monolayers, one can tune E_d by interchanging side groups, as studied experimentally in Ref. [74] and theoretically in Ref. [75]. Tuning E_d *in situ* is more difficult. Note that

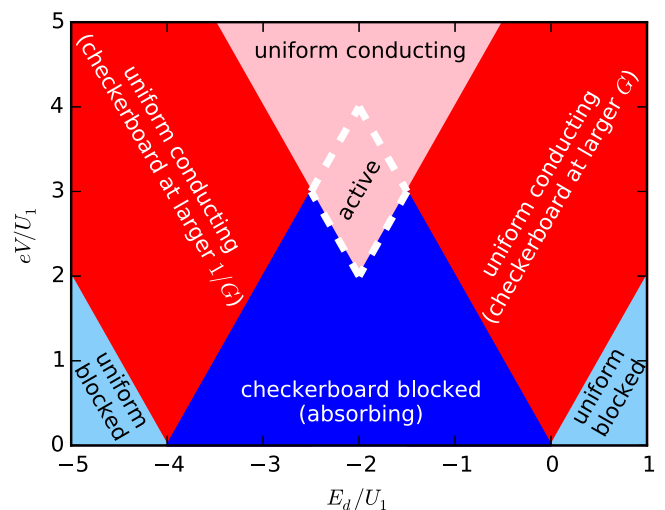


FIG. 10. Phase diagram obtained from Monte Carlo simulations for the monolayer with degeneracy $G = 2$ and temperature $T = 0$. Compare the MFME phase diagram in Fig. 4. In the region marked “active,” the layer is in the uniform conducting state even though the two states with perfect checkerboard charge order (and no current) are absorbing.

tuning E_d and V is equivalent to changing the potential drops between the molecules and the two electrodes independently. This could be done by asymmetrically changing the molecule-electrode distances: If the molecules are covalently bound to one electrode but only van der Waals coupled to the other, changing the electrode-electrode separation would have the desired effect. This would of course also change the tunneling amplitudes.

We now present simulation results for the most relevant observables in the stationary state for $G = 2$, corresponding to pure spin degeneracy of the occupied sites. The average imbalance between the occupation numbers per site on the two sublattices $\langle |n_A - n_B| \rangle$ is shown in Fig. 11, the average occupation in Fig. 12, and the average current in Fig. 13. As discussed before, there is a uniform fully occupied phase for $E_d/U_1 < -4$, a corresponding uniform completely empty phase for $E_d/U_1 > 0$, and a perfectly checkerboard-ordered phase in-between. All of them are blocking the current due to the absence of allowed transitions in the bias window. For increasing bias, the monolayer will eventually become conducting and disordered as more and more transitions enter the bias window. Note that $\langle |n_A - n_B| \rangle$ is not identically zero in the conducting phases since the nonzero current implies fluctuations in the occupation numbers. All three quantities plotted in Figs. 11–13 clearly show a double-peaked blocked region resulting from the appearance of an active phase in region (4,1) (see Fig. 2). The current and the average occupation approach and finally reach the noninteracting single-site limit as the number of transitions in the bias window is increased. The observables are asymmetric in the onsite energy relative to $E_d/U_1 = -2$ since the degeneracy $G = 2$ breaks particle-hole symmetry.

It would be desirable to verify the checkerboard charge order experimentally. The charge order implies the presence of two populations of molecules or quantum dots with distinct average charge, each comprising 50% of the monolayer. In the blocked phase, charge fluctuations are suppressed. For

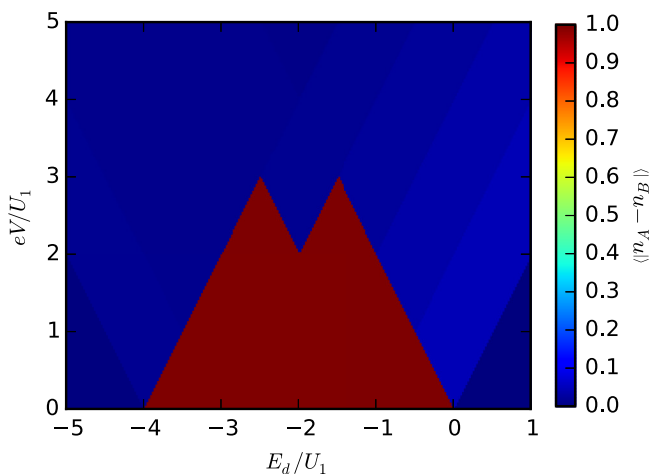


FIG. 11. Monte Carlo results for the average imbalance between the occupation numbers per site on the two sublattices $\langle |n_A - n_B| \rangle$, for $T = 0$, $L = 64$, and $G = 2$. In the central region, the system ends up in one of the two absorbing checkerboard-ordered states so that the order parameter is exactly $\frac{1}{2}$.

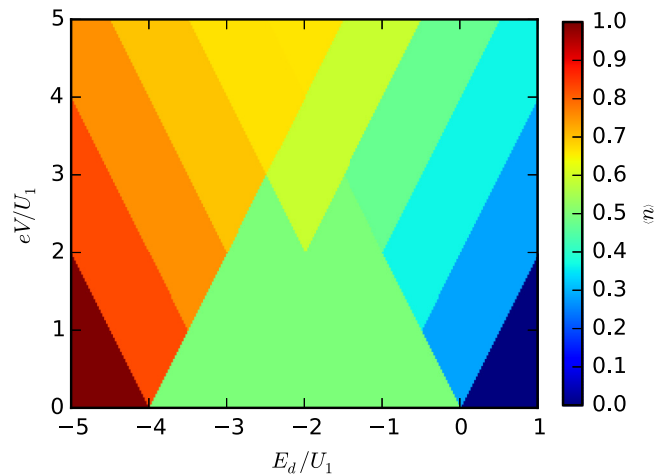


FIG. 12. Monte Carlo results for the average occupation per site $\langle n \rangle$ for the same parameters as in Fig. 11. The occupation is 0 and 1 in the regions (0,0) and (5,5), respectively, and $\frac{1}{2}$ in the checkerboard-ordered region. The average occupation assumes a nonuniversal value in the other regions, which grows for smaller onsite energy E_d and tends toward $G/(G + 1) = \frac{2}{3}$ for increasing bias voltage V .

molecular layers, the resulting equal distribution of charge states could be seen by optical spectroscopy, for example, in reflection geometry with a transparent conductor as top electrode. On the other hand, in the checkerboard conducting phase, the occupation number of one population fluctuates due to the current, whereas the other is essentially fixed. Spectroscopy should thus see two charge states but with different probabilities. For a layer of metallic nanoparticles, one could similarly try to observe the presence of two populations with distinct surface-plasmon frequencies. A more challenging idea is to observe the diffraction pattern due to the diffraction grating formed by the charge density wave.

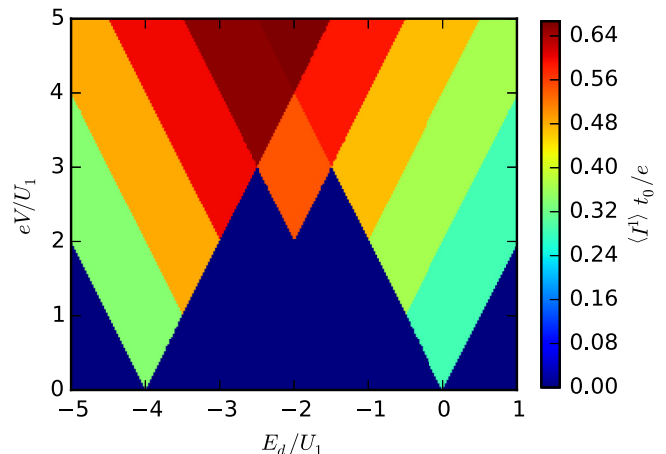


FIG. 13. Monte Carlo results for the average current per site through the lead $\alpha = 1$ [Eq. (9)] for the same parameters as in Fig. 11. The current vanishes in the absorbing phases and grows with the number of transitions in the bias window, i.e., with the bias voltage V .

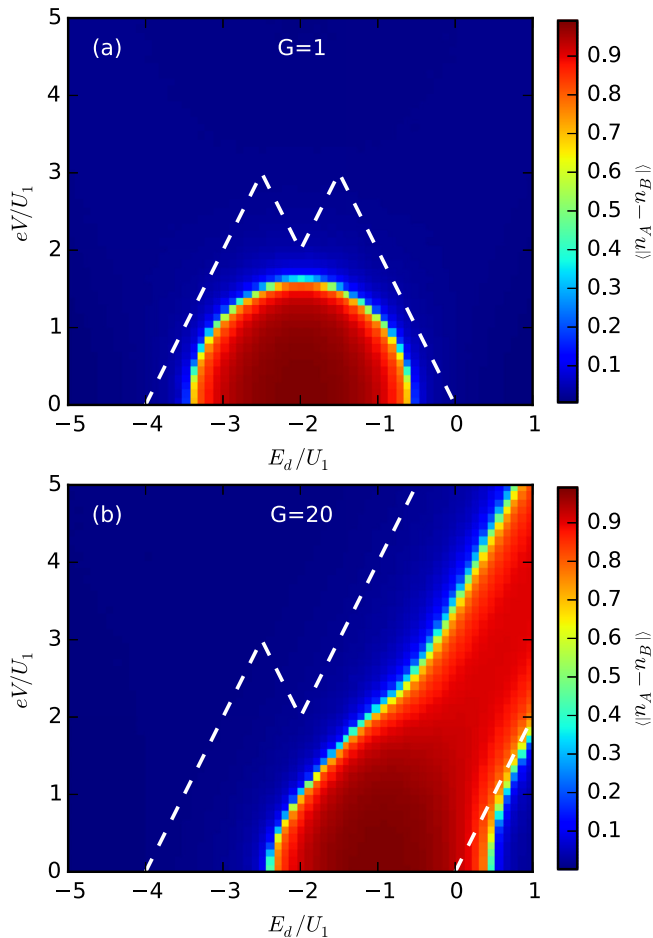


FIG. 14. Checkerboard order parameter $\langle |n_A - n_B| \rangle$ from Monte Carlo simulations for $T/U_1 = 0.35$ and $L = 64$. The degeneracy is (a) $G = 1$ and (b) $G = 20$. The dashed lines denote the boundary between the checkerboard-ordered and uniform phases for $T = 0$. Note that even though the temperature is a sizable fraction of the zero-field critical temperature of the Ising model, the large degeneracy in panel (b) still stabilizes the checkerboard conducting phase.

IV. RESULTS FOR NONZERO TEMPERATURES

In this section, we present results for nonzero temperatures. While this is clearly required for comparison with experiments, the case of $T > 0$ is less interesting from the point of view of statistical physics. The nontrivial DP2 transition found for $T = 0$ in Sec. III D relies on the perfect checkerboard states being absorbing, which is no longer the case for $T > 0$. Hence, we expect all (equilibrium and nonequilibrium) phase transitions to be in the 2D Ising universality class [40]. This also holds for those transitions that were trivially discontinuous for $T = 0$ due to the jump in the Fermi function. At $T > 0$, the Fermi functions and consequently the transition rates $R_{i \rightarrow f}$ in Eq. (6) are continuous functions of the parameters E_d/U_1 , eV/U_1 , and T/U_1 .

Figure 14 shows results for the checkerboard order parameter for a temperature of approximately two thirds of the Ising critical temperature $T_c \approx 0.567 U_1$ and two values of G , the particle-hole symmetric case $G = 1$ and the large degeneracy $G = 20$. The observed shrinking of the regime

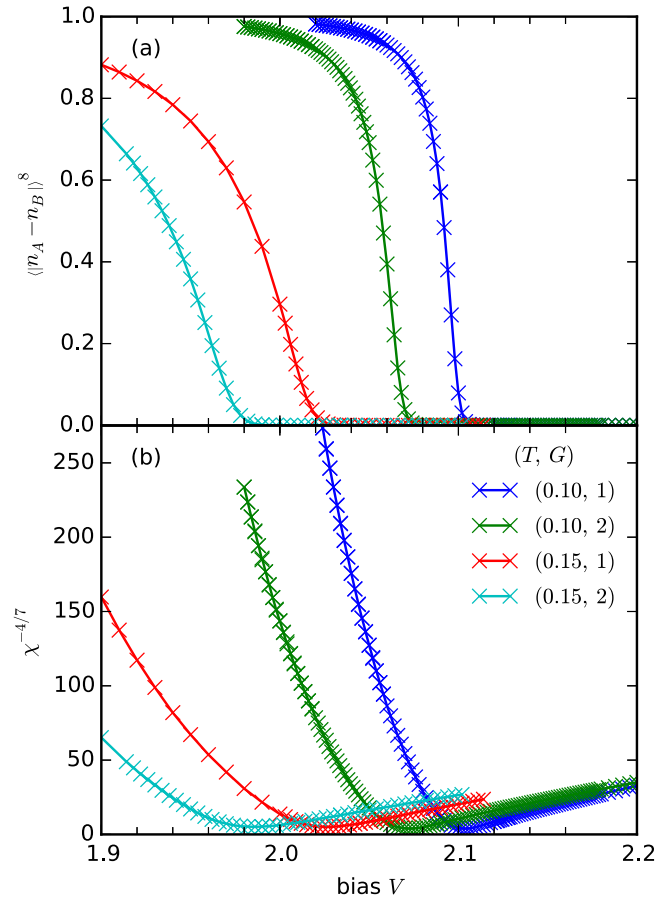


FIG. 15. Monte Carlo results for (a) the checkerboard order parameter $\langle |n_A - n_B| \rangle$ to the power 8 and (b) the corresponding susceptibility to the power $-\frac{4}{7}$ as functions of the bias voltage V for various values of G and T . The remaining parameters are $E_d/U_1 = 2.2$ and $L = 64$. The results are consistent with the 2D Ising universality class.

with checkerboard order compared to $T = 0$ is of course expected since higher temperatures allow additional tunneling processes that tend to destabilize charge order. For $G = 20$, the ordered regime is also shifted to larger E_d , in accordance with the effective onsite energy $E_d - T \ln G$ (see Sec. III C). Interestingly, for this large value of G , the checkerboard conducting phase is found to be rather robust against thermal fluctuations.

The character of the phase transitions can obviously not be inferred from Fig. 14. We exemplarily consider the transition between checkerboard and uniform phases driven by the bias voltage V at a fixed onsite energy E_d and several values of T and G . As in Sec. III C, we plot the checkerboard order parameter to the power 8 and the corresponding susceptibility to the power $-\frac{4}{7}$ in Fig. 15. The results are consistent with the 2D Ising universality class [40,60,65].

We finally turn to the checkerboard conducting regions, specifically the region (1,0), at nonzero temperatures. We found in Sec. III C that at $T = 0$ there is a transition between uniform and checkerboard-ordered conducting states as the degeneracy G is increased. For this, it is important that a checkerboard state cannot be destroyed by electrons tunneling in to create occupied defects in the empty sublattice since

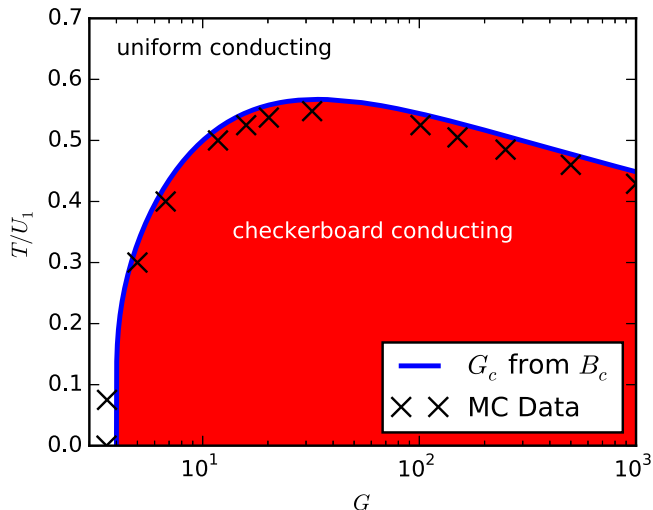


FIG. 16. Phase diagram in the G - T plane for $eV/U_1 = E_d/U_1 = 0$, i.e., in region (1,0). The crosses denote the location of the phase transition determined from the maximum of the susceptibility χ obtained from Monte Carlo simulations for $L = 64$. The continuous line is based on the conjecture for the critical magnetic field in Ref. [61].

the corresponding rate vanishes. This is no longer true for $T > 0$; for low temperatures there is now an exponentially small rate for creating such occupied defects. However, this in-tunneling rate contains a factor of G so that for increasing G the checkerboard state should eventually be destabilized in favor of a uniform state with occupancy close to unity. The same conclusion is reached by considering the effective onsite energy $E_d - T \ln G$ in the equivalent Ising model. This expectation is indeed borne out by the results presented in Fig. 16. We find a reentrant transition to the uniform conducting state at large G , which shifts to smaller G for increasing temperature. On the other hand, the transition to checkerboard order at lower G shifts upwards with temperature. Both trends are consistent with the expectation that higher temperatures disfavor ordering. Above the corresponding critical temperature of the 2D Ising model, checkerboard order does not exist for any G . Since Fig. 16 shows results for $V = 0$, i.e., in equilibrium, the critical temperature versus G should map to the critical temperature versus applied magnetic field for the Ising model. Our simulation results indeed agree well with the conjecture of Müller-Hartmann and Zittartz [61].

V. SUMMARY AND CONCLUSIONS

In summary, we have studied a square lattice of quantum dots or molecules under a bias voltage applied perpendicular to the layer. We have assumed infinite onsite repulsion and finite nearest-neighbor Coulomb interaction within the layer, as well as vanishing intralayer hopping and weak monolayer-electrode hopping. The indirect hopping from a site in the monolayer to one of the electrodes and further to a *different* site of the monolayer is assumed to be fully incoherent, which is the case in the limits of short Fermi wavelength or strong disorder in the electrodes. By employing Monte Carlo simulations, we avoid mean-field approximations. The interactions lead

to the appearance of charge-density-wave phases. Apart from the charge order, the main quantity of interest is the current perpendicular to the layer.

The resulting zero-temperature phase diagram, Fig. 10, shows blocked phases with vanishing current and zero, single, or checkerboard-ordered occupancy. The latter can be understood as a Coulomb-blockade state induced by the nearest-neighbor repulsion. These phases are connected to an equilibrium Ising model at $V = 0$. At larger bias voltages, they give way to conducting phases. Interestingly, it is possible for these phases to possess checkerboard charge order. This requires a high degeneracy $G \gtrsim 3.6$ of the occupied single-site states, which could be realized by combining charge and orbital degeneracies. The transition between the uniform conducting phase and the checkerboard conducting phase as a function of G is in the 2D Ising universality class. The checkerboard conducting phase only exists out of equilibrium. In a large parameter range we find a transition from a uniform blocked phase to a checkerboard conducting phase at a finite critical bias voltage. This constitutes an interesting case of bias- or current-induced charge order. Furthermore, there is a region at finite bias voltage for which the two symmetry-related blocked checkerboard states are absorbing but the stationary state is nevertheless conducting and uniform. The presence of this active phase is evident in the current-voltage characteristics. It is interesting that such an active phase could be realized in a monolayer under bias, as there are not many experimental realizations. By judiciously taking the limit $T \rightarrow 0$, we determine the phase transition between the absorbing and active phases to be in the 2D DP2 universality class.

The features found at $T = 0$ are robust for small nonzero temperatures, except that absorbing states no longer exist for $T > 0$ and that, as a consequence, the absorbing-to-active phase transition transforms into a 2D Ising transition between checkerboard blocked and uniform conducting phases. Apart from this change, the ordered phases shrink and, for degeneracies $G > 1$, shift to higher onsite energies for increasing temperature.

It would be desirable to extend the underlying dynamics to contain coherences as well as higher-order tunneling processes such as cotunneling and pair tunneling. Even in the absence of intralayer hopping, tunneling via the electrodes can induce coherences between eigenstates of the local particle numbers, i.e., delocalized charges in the monolayer. Intralayer hopping of course also favors delocalization in the monolayer. Higher-order processes and coherences are required for a study of Kondo-type effects in tunneling through the layer. Coherent hopping, be it direct or indirect through the electrodes, would turn the system into a much more difficult extended Hubbard model out of equilibrium. This would call for nonequilibrium *quantum* Monte Carlo simulations, which would suffer from the sign problem. On the other hand, a higher-order MFME including coherences seems feasible. In any case, even the quasiclassical model considered here should be valuable for further studies. On the one hand, comparison with experiments, for example, on rolled-up structures, calls for a realistic description of electronic, spin, and vibrational degrees of freedom of molecular layers. On the other, further studies of the considered model might help to constrain the critical behavior of the 2D DP2 universality class.

ACKNOWLEDGMENTS

We would like to thank S. Diehl, J. Marino, A. Rubio, T. Vojta, and A. Wacker for useful discussions. Financial support by the Deutsche Forschungsgemeinschaft, through

Research Unit FOR 1154, *Towards Molecular Spintronics*, is gratefully acknowledged. C.T. also acknowledges support by the Deutsche Forschungsgemeinschaft through Collaborative Research Center SFB 1143.

-
- [1] I. E. Itskevich, T. Ihn, A. Thornton, M. Henini, T. J. Foster, P. Moriarty, A. Nogaret, P. H. Beton, L. Eaves, and P. C. Main, *Phys. Rev. B* **54**, 16401 (1996).
- [2] M. Narihiro, G. Yusa, Y. Nakamura, T. Noda, and H. Sakaki, *Appl. Phys. Lett.* **70**, 105 (1997).
- [3] T. Suzuki, K. Nomoto, K. Taira, and I. Hase, *Jpn. J. Appl. Phys.* **36**, 1917 (1997).
- [4] I. Hapke-Wurst, U. Zeitler, H. W. Schumacher, R. J. Haug, K. Pierz, and F. J. Ahlers, *Semicond. Sci. Technol.* **14**, L41 (1999).
- [5] A. Belyaev, L. Eaves, S. Vitusevich, P. Main, M. Henini, A. Förster, N. Klein, and S. Danylyuk, in *Proceedings of the 25th International Conference on the Physics of Semiconductors (ICPS 25)*, edited by N. Miura (Springer, Berlin, 2001).
- [6] I. Hapke-Wurst, U. Zeitler, U. F. Keyser, R. J. Haug, K. Pierz, and Z. Ma, *Appl. Phys. Lett.* **82**, 1209 (2003).
- [7] S. D. Lin and C. P. Lee, *J. Appl. Phys.* **93**, 2952 (2003).
- [8] F. Pulizzi, E. E. Vdovin, K. Takehana, Y. V. Dubrovskii, A. Patané, L. Eaves, M. Henini, P. N. Brunkov, and G. Hill, *Phys. Rev. B* **68**, 155315 (2003).
- [9] D. Austing, R. Hill, A. Patané, P. Main, M. Henini, L. Eaves, and S. Tarucha, *Phys. E (Amsterdam)* **26**, 482 (2005).
- [10] J. Sun, P. Jin, C. Zhao, L. Yu, X. Ye, B. Xu, Y. Chen, and Z. Wang, *J. Electrochem. Soc.* **153**, G703 (2006).
- [11] E. E. Vdovin, Y. N. Khanin, O. Makarovskiy, Y. V. Dubrovskii, A. Patané, L. Eaves, M. Henini, C. J. Mellor, K. A. Benedict, and R. Airey, *Phys. Rev. B* **75**, 115315 (2007).
- [12] I. Swart, P. Liljeroth, and D. Vanmaekelbergh, *Chem. Rev.* **116**, 11181 (2016).
- [13] W. C. Bigelow, D. L. Pickett, and W. A. Zisman, *J. Colloid Sci.* **1**, 513 (1946).
- [14] M. Scheffler, L. Smykalla, D. Baumann, R. Schlegel, T. Hänke, M. Toader, B. Büchner, M. Hietschold, and C. Hess, *Surf. Sci.* **608**, 55 (2013).
- [15] L. Smykalla, P. Shukryna, M. Korb, H. Lang, and M. Hietschold, *Nanoscale* **7**, 4234 (2015).
- [16] G. E. Poirier, M. J. Tarlov, and H. E. Rushmeier, *Langmuir* **10**, 3383 (1994).
- [17] D. Vuillaume, C. Boullas, J. Collet, J. V. Davidovits, and F. Rondelez, *Appl. Phys. Lett.* **69**, 1646 (1996).
- [18] G. M. Whitesides and M. Boncheva, *Proc. Natl. Acad. Sci. USA* **99**, 4769 (2002).
- [19] S. Lodha and D. B. Janes, *Appl. Phys. Lett.* **85**, 2809 (2004).
- [20] V. Prinz, V. Seleznev, A. Gutakovskiy, A. Chehovskiy, V. Preobrazhenskii, M. Putyato, and T. Gavrilova, *Phys. E (Amsterdam)* **6**, 828 (2000).
- [21] O. G. Schmidt and K. Eberl, *Nature (London)* **410**, 168 (2001).
- [22] C. C. Bof Bufon, C. Vervacke, D. J. Thurmer, M. Fronk, G. Salvan, S. Lindner, M. Knupfer, D. R. T. Zahn, and O. G. Schmidt, *J. Phys. Chem. C* **118**, 7272 (2014).
- [23] C. C. Bof Bufon, J. D. Cojal González, D. J. Thurmer, D. Grimm, M. Bauer, and O. G. Schmidt, *Nano Lett.* **10**, 2506 (2010); D. J. Thurmer, C. C. Bof Bufon, C. Deneke, and O. G. Schmidt, *ibid.* **10**, 3704 (2010); C. C. Bof Bufon, J. D. Arias Espinoza, D. J. Thurmer, M. Bauer, C. Deneke, U. Zschieschang, H. Klauk, and O. G. Schmidt, *ibid.* **11**, 3727 (2011); C. Müller, C. C. Bof Bufon, M. E. Navarro Fuentes, D. Makarov, D. H. Mosca, and O. G. Schmidt, *Appl. Phys. Lett.* **100**, 022409 (2012); D. Grimm, C. C. Bof Bufon, C. Deneke, P. Atkinson, D. J. Thurmer, F. Schäffel, S. Gorantla, A. Bachmatiuk, and O. G. Schmidt, *Nano Lett.* **13**, 213 (2013).
- [24] A. Vilan, A. Shanzer, and D. Cahen, *Nature (London)* **404**, 166 (2000).
- [25] A. Vilan and D. Cahen, *Adv. Funct. Mater.* **12**, 795 (2002).
- [26] N. Stein, R. Korobko, O. Yaffe, R. H. Lavan, H. Shpaisman, E. Tirosh, A. Vilan, and D. Cahen, *J. Phys. Chem. C* **114**, 12769 (2010).
- [27] M. Tian, J. Wang, J. Kurtz, T. E. Mallouk, and M. H. W. Chan, *Nano Lett.* **3**, 919 (2003).
- [28] M. Coll, L. H. Miller, L. J. Richter, D. R. Hines, O. D. Jurchescu, N. Gergel-Hackett, C. A. Richter, and C. A. Hacker, *J. Am. Chem. Soc.* **131**, 12451 (2009).
- [29] G. Wang, Y. Kim, M. Choe, T.-W. Kim, and T. Lee, *Adv. Mater.* **23**, 755 (2011).
- [30] D. Vuillaume, in *Oxford Handbook of Nanoscience and Technology*, edited by A. Narlikar and Y. Fu (Oxford University Press, Oxford, UK, 2010), Vol. 3, Chap. 9, pp. 312–342.
- [31] S. Andergassen, V. Meden, H. Schoeller, J. Splettstoesser, and M. R. Wegewijs, *Nanotechnology* **21**, 272001 (2010).
- [32] H. Bruus and K. Flensberg, *Many-Body Quantum Theory in Condensed Matter Physics* (Oxford University Press, Oxford, UK, 2004).
- [33] P. C. Hohenberg and B. I. Halperin, *Rev. Mod. Phys.* **49**, 435 (1977).
- [34] M. C. Cross and P. C. Hohenberg, *Rev. Mod. Phys.* **65**, 851 (1993).
- [35] H. Hinrichsen, *Adv. Phys.* **49**, 815 (2000).
- [36] G. Ódor, *Rev. Mod. Phys.* **76**, 663 (2004).
- [37] G. Kießlich, A. Wacker, and E. Schöll, *Phys. B (Amsterdam)* **314**, 459 (2002); G. Kießlich, A. Wacker, E. Schöll, S. A. Vitusevich, A. E. Belyaev, S. V. Danylyuk, A. Förster, N. Klein, and M. Henini, *Phys. Rev. B* **68**, 125331 (2003).
- [38] R. Wetzler, A. Wacker, and E. Schöll, *Phys. Rev. B* **68**, 045323 (2003); R. Wetzler, R. Kunert, A. Wacker, and E. Schöll, *New J. Phys.* **6**, 81 (2004).
- [39] M. Leijnse, *Phys. Rev. B* **87**, 125417 (2013).
- [40] A. Mitra, S. Takei, Y. B. Kim, and A. J. Millis, *Phys. Rev. Lett.* **97**, 236808 (2006).
- [41] H. Bolvin and O. Kahn, *Chem. Phys.* **192**, 295 (1995); *Chem. Phys. Lett.* **243**, 355 (1995).
- [42] A. Bousseksou, H. Constant-Machado, and F. Varret, *J. Phys. I (France)* **5**, 747 (1995).

- [43] T. Yokoyama, Y. Murakami, M. Kiguchi, T. Komatsu, and N. Kojima, *Phys. Rev. B* **58**, 14238 (1998).
- [44] H.-P. Breuer and F. Petruccione, *The Theory of Open Quantum Systems* (Oxford University Press, Oxford, UK, 2007).
- [45] C. Timm, *Phys. Rev. B* **77**, 195416 (2008).
- [46] R. K. Wangsness and F. Bloch, *Phys. Rev.* **89**, 728 (1953).
- [47] F. Bloch, *Phys. Rev.* **105**, 1206 (1957).
- [48] A. G. Redfield, *Adv. Magn. Reson.* **1**, 1 (1965).
- [49] G. C. Wick, A. S. Wightman, and E. P. Wigner, *Phys. Rev.* **88**, 101 (1952); *Phys. Rev. D* **1**, 3267 (1970).
- [50] W. H. Zurek, *Phys. Rev. D* **26**, 1862 (1982).
- [51] D. Giulini, C. Kiefer, and H. Zeh, *Phys. Lett. A* **199**, 291 (1995).
- [52] F. Elste and C. Timm, *Phys. Rev. B* **71**, 155403 (2005).
- [53] C. Timm, *Phys. Rev. B* **83**, 115416 (2011).
- [54] Kinetic simulations would require us to advance the simulation time by an exponentially distributed time with this mean. However, for the long-time limit we are interested in, both prescriptions give the same results.
- [55] A. Bortz, M. Kalos, and J. Lebowitz, *J. Comput. Phys.* **17**, 10 (1975).
- [56] D. T. Gillespie, *J. Comput. Phys.* **22**, 403 (1976); *J. Phys. Chem.* **81**, 2340 (1977).
- [57] T. P. Schulze, *Phys. Rev. E* **65**, 036704 (2002).
- [58] R. H. Swendsen and J.-S. Wang, *Phys. Rev. Lett.* **57**, 2607 (1986).
- [59] U. Wolff, *Phys. Rev. Lett.* **62**, 361 (1989).
- [60] R. K. Pathria and P. D. Beale, *Statistical Mechanics*, 3rd ed. (Elsevier/Academic, New York, 2011).
- [61] E. Müller-Hartmann and J. Zittartz, *Z. Phys. B* **27**, 261 (1977).
- [62] G. D. Mahan and F. H. Claro, *Phys. Rev. B* **16**, 1168 (1977).
- [63] One might ask whether the rate equations really describe relaxation into these ground states. This is the case if we set $V = 0$ and then take the limit $T \rightarrow 0$ since the system is ergodic for any $T > 0$.
- [64] H. W. J. Blöte and M. P. M. den Nijs, *Phys. Rev. B* **37**, 1766 (1988).
- [65] L. M. Sieberer, S. D. Huber, E. Altman, and S. Diehl, *Phys. Rev. Lett.* **110**, 195301 (2013); *Phys. Rev. B* **89**, 134310 (2014).
- [66] Raising G also increases the rate for creating an occupied defect on the empty sublattice, which destabilizes the order, but for this to happen more than one empty defect at neighboring sites is needed, which makes the overall creation rate of such defects much smaller than the overall rate for removing empty defects.
- [67] R. A. Ferrell, N. Menyh ard, H. Schmidt, F. Schwabl, and P. Sz epfalusy, *Phys. Rev. Lett.* **18**, 891 (1967); R. Ferrell, N. Menyh ard, H. Schmidt, F. Schwabl, and P. Sz epfalusy, *Ann. Phys. (NY)* **47**, 565 (1968).
- [68] B. I. Halperin and P. C. Hohenberg, *Phys. Rev.* **177**, 952 (1969).
- [69] P. Grassberger and A. de la Torre, *Ann. Phys. (NY)* **122**, 373 (1979).
- [70] M. A. Mu oz, G. Grinstein, and Y. Tu, *Phys. Rev. E* **56**, 5101 (1997).
- [71] M. Y. Lee and T. Vojta, *Phys. Rev. E* **83**, 011114 (2011).
- [72] H. Hinrichsen, *Phys. Rev. E* **55**, 219 (1997).
- [73] I. Dornic, H. Chat e, J. Chave, and H. Hinrichsen, *Phys. Rev. Lett.* **87**, 045701 (2001).
- [74] L. Venkataraman, Y. S. Park, A. C. Whalley, C. Nuckolls, M. S. Hybertsen, and M. L. Steigerwald, *Nano Lett.* **7**, 502 (2007).
- [75] D. J. Mowbray, G. Jones, and K. S. Thygesen, *J. Chem. Phys.* **128**, 111103 (2008).